Composites: Part A 204 (2026) 109641

Contents lists available at ScienceDirect

Composites Part A

journal homepage: www.elsevier.com/locate/compositesa

Low earth orbit environment effects on shape memory phthalonitrile resins

Rongxiang Hu [a], Fenghua Zhang [a], Yanju Liu [b], Liwu Liu [b], Zhengxian Liu [a], Jinsong Leng [a,*]

[a] Centre for Composite Materials and Structures, Harbin Institute of Technology (HIT), Harbin 150080, PR China
[b] Department of Astronautical Science and Mechanics, Harbin Institute of Technology (HIT), Harbin 150001, PR China

HIGHLIGHTS

- The damage behavior of shape memory phthalonitrile resin in LEO is first reported.
- The resin retains stable fundamental properties after space exposure.
- Gradient damage of curved surfaces was revealed in the space environment.

GRAPHICAL ABSTRACT

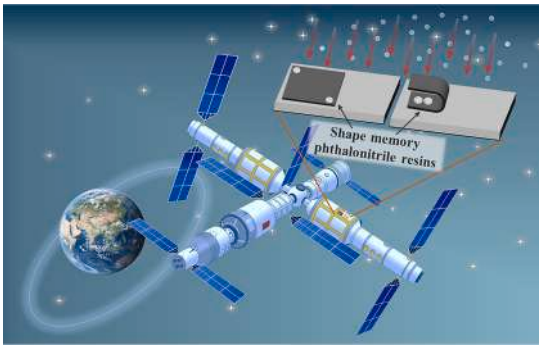

ARTICLE INFO

Keywords:
Smart materials
Environmental degradation
Microstructural analysis

ABSTRACT

Shape memory phthalonitrile (SMPN) resins have been exposed in low Earth orbit (LEO) environment aboard the China Space Station (CSS). The exposure experiment included one SMPN sample in its original flat shape and another in a temporary "U" shape. After exposure, the mass loss rate of the SMPN remains below 6.5%. Although SEM revealed severe surface erosion to a depth of approximately 28 μm and FTIR indicated damage to the aliphatic segment of SMPN, the results of nanoindentation, DMA, and TGA tests show that the fundamental properties of the exposed SMPN remained largely unaffected. It is worth noting that the SMPN sample with a temporary "U" shape still retained its temporary shape after exposure and could recover its original shape upon thermal stimulation, achieving a shape recovery rate of approximately 97%. Microstructural analysis of the recovery sample indicates that the outer surface of the exposed U-shaped SMPN displays gradient damage characteristics, which could inform the optimization of damage-resistant designs in spacecraft structures. Despite the surface erosion, this study demonstrates that the SMPN maintains stable performance after space exposure, indicating its potential to serve as a material suitable for space environments.

1. Introduction

Shape memory polymers (SMPs) are smart materials capable of recovering from a temporary shape to their original shape in response to external stimuli such as heat, light, electricity, or magnetic fields [1–4]. Owing to their programmable shape, strong responsiveness to external

* Corresponding author.
E-mail address: lengjs@hit.edu.cn (J. Leng).

https://doi.org/10.1016/j.compositesa.2026.109641
Received 10 November 2025; Received in revised form 22 January 2026; Accepted 5 February 2026
Available online 6 February 2026

stimuli, and lightweight, SMPs have demonstrated broad application prospects in the aerospace field, particularly in deployable structures and flexible spacecraft components, and hold great potential to replace traditional mechanical unfolding systems [5–7]. However, the space environment is extremely complex and harsh, particularly in low Earth orbit (LEO), where materials are subjected to high vacuum, atomic oxygen (AO), strong ultraviolet (UV) radiation, high-energy particle irradiation, and extensive thermal cycling [8–10]. Prolonged exposure to the space environment can lead to significant degradation of the optical, thermal and mechanical properties, ultimately compromising the reliability of the spacecraft materials.

Although the performance of materials can be preliminarily evaluated through ground-based simulation, the complexity of the actual space environment makes it difficult for such experiments to accurately reflect the long-term service behavior of materials in orbit. With the advancement of space station construction, conducting exposure experiments in orbit has become a reliable approach for investigating the performance evolution of materials under space environmental conditions. Since 2001, NASA has continuously conducted the Materials International Space Station Experiment (MISSE) missions on the exterior of the International Space Station (ISS), involving the exposure of various materials such as polyimides (PI), polyethylene terephthalate (PET), liquid crystal polymers (LCPs), shape memory polymer composites (SMPC), and 3D printed carbon fiber composites [11–14]. Subsequently, the European Space Agency (ESA) and the Japan Aerospace Exploration Agency (JAXA) have also carried out a range of material exposure experiments on the ISS [15–17]. The implementation of space exposure experiments has significantly advanced the understanding of how the space environment affects material properties.

With the rapid advancement of space exploration and space station construction, the China Space Station (CSS) has entered a stage of normalized operation and has been conducting exposure experiments in space [18–21]. In this study, shape memory phthalonitrile resin (SMPN), one of the materials exposed on the CSS, is discussed. It contains one original flat sample and one sample with a temporary “U” shape. The samples were delivered to the space station on November 12, 2022, and were deployed for space exposure on March 8, 2023. After one year, the materials were retrieved from the exposure cabin in March 2024 and transferred into the space station for storage. Due to the limited space resources of the cargo spacecraft, the flat SMPN sample was returned to Earth together with the panel containing the flat samples in May 2024, whereas the U-shaped SMPN sample was packaged and sealed with the corresponding panel and was not returned to Earth until March 2025.

2. Material and methods

2.1. Preparation of samples for LEO environment exposure experiments

The preparation method of the SMPN has been previously reported, involving the use of monomers and end-capping agents, followed by high-temperature curing under the catalytic action of aromatic amines [22]. The cured SMPN was fabricated into a flat sample with dimensions of 36 × 33.5 × 2 mm, and another piece was processed into a 45 × 12 × 2 mm specimen and deformed into a temporary “U” shape. The samples were categorized and mounted on separated metal plates, which were then carried to the CSS aboard the Tianzhou-5 spacecraft. During the exposure experiment, the samples were placed outside the cabin.

2.2. Testing and characterization of space retrieved samples

After samples retrieval, the exposed SMPN surface was characterized using a 3D Ultra Depth of Field Microscope (VHX-7000 N, KEYENCE). Subsequently, the flat samples were divided into multiple parts for different tests. Scanning electron microscope (SEM) was performed using a TESCAN AMBER, Fourier transform infrared (FTIR) spectroscopy was conducted using an INVENIO S (Bruker), and X-ray photoelectron spectroscopy (XPS) was carried out on AXIS Supar+ (Shimadzu). X-ray Diffraction (XRD) analysis was performed using a Rigaku Ultima IV diffractometer. Nanoindentation testing was conducted using UNHT (Anton Paar) with a maximum indentation depth of 200 nm. Dynamic mechanical analysis (DMA) was conducted using a DMA Q800 (TA Co., America) in multi-frequency strain mode at a constant frequency of 1 Hz, with a temperature ramp from 25 °C to 400 °C at a rate of 5 °C min^{-1}.Thermogravimetric analysis (TGA) was performed using a TGA/DSC 1 STAR^e System (METTLER TOLEDO) under a nitrogen atmosphere, with heating from 25 °C to 1000 °C at a rate of 10 °C /min.

2.3. Fabrication of composites

Carbon fiber (CF) reinforced SMPN composites were fabricated via prepolymer impregnation followed by hot-press curing. The CF used for composite was T300-type twill fabric purchased from Toray Industries. The prepolymer, consisting of the monomer, end-capping agent, and curing agent, was dissolved in N, N-dimethylformamide to form a homogeneous solution, which was subsequently used to impregnate the CF fabrics, with the solid content of the resin was about 50%. The impregnated fabrics were subjected to stepwise heating at 100 °C for 1 h, 150 °C for 30 min, and 200 °C for 15 min to remove the solvent, yielding SMPN-based composite prepregs. The resulting prepregs were then compacted and followed by gradient thermal curing in a high-temperature oven according to the following protocol: 220 °C for 2 h, 260 °C for 4 h, 280 °C for 4 h, 300 °C for 4 h, 325 °C for 4 h, and 350 °C for 4 h, to obtain CF reinforced SMPN based composites (SMPNC). The composite containing one, two, and three layers of CF were prepared and denoted as SMPNC1, SMPNC2, and SMPNC3, respectively.

3. Results

3.1. Surface morphology evolution

Table 1 presents the mass changes of the material before and after space exposure. After 12 months of exposure, the weight of flat SMPN was 1325.0 mg, with a mass loss of approximately 6.36%, while the U-shaped SMPN exhibited a mass loss of about 3.05%. The mass loss ratio of the flat sample was higher than that of the U-shaped sample, which is mainly attributed to its larger surface directly exposed to various space damage. The erosion rate of exposed flat SMPN sample was calculated according to the reference report [23], resulting in a value of approximately 1.19 × 10^{-24} cm^2/atoms. In comparison with those polymers exposed on the ISS, SMPN shows a relatively lower erosion rate, and the corresponding comparative data are provided in the supporting information. However, the material lost from SMPN in the space environment can be released in other forms, such as decomposition gases or erosion generated particles, which may interfere with precision optical instruments. Therefore, before this potential risk is fully eliminated, the application of SMPN in structures located near optical devices should be considered with caution.

Fig. 1 shows the digital images of the flat SMPN sample. Fig. 1a displays an image of the samples taken on the ground before the exposure experiment. Fig. 1 shows the opening process of the storage box containing the exposed samples after the completion of the exposure experiment and their retrieval to the space station, and Fig. 1b presents a

Table 1
Mass losses of samples after exposure.

Parameter	Flat sample	U-shaped sample
Sample size	36 × 33.5 × 2 mm	45 × 12 × 2 mm
Original weight	1415.0 mg	642.8 mg
Weight after exposure	1325.0 mg	623.2 mg
Weight loss ratio	6.36%	3.05%

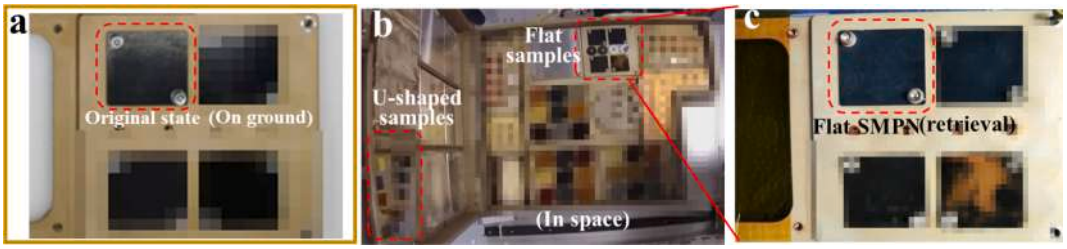

Fig. 1. Digital image of (a) the flat SMPN sample on the ground, (b) the exposure samples in the space station, (c) the exposure SMPN sample after retrieval.

snapshot of the opening process. Fig. 1c shows a digital photograph of the exposed sample after its return to Earth. The surface of the SMPN after exposure appears rough, and its microstructure is charactered subsequently.

As a control, the surface morphology of the original SMPN was examined using SEM. Fig. 2a shows that the original surface is smooth and flat, except for minor processing marks introduced during fabrication. Fig. 2b present the magnified views of the exposed SMPN sample. Due to prolonged exposure to AO and various types of cosmic radiation, the surface exhibits a rough texture. Fig. 2c presents the image taken by 3D ultra depth of field microscope of the same area. The sample surface displays height variations, with the central region being relatively lower than the surrounding areas. This may be attributed to the uneven distribution of AO and charged particles and so on in the space environment, which leads to intensified local erosion. Since this region is located near the center of the observation area, it results in the observed morphology.

The microstructure of the surface was further characterized by SEM. Fig. 2d shows that the surface of the exposed SMPN has undergone significant erosion, resulting in a dense microporous structure. Upon higher magnification observation, Fig. 2e reveals that the numerous tiny erosion pits almost entirely cover the observed area, which can be attributed to the harsher exposure to cosmic radiation, AO, and charged particles. Actually, this surface morphology of exposed SMPN is similar to that of exposed polymer such as PI and fluorinated ethylene propylene after atomic oxygen erosion aboard the ISS [23]. The cross-sectional morphology of the SMPN, as shown in Fig. 2f, exhibits vertical erosion, with the affected depth reaching up to 28 μm. The results demonstrate that the surface of SMPN suffer from serious erosion in space environment, which is similar to that observed in other exposed polymers eroded by atomic oxygen in LEO.

3.2. Surface chemical structure evolution

Fig. 3a illustrates the monomer structures of the raw materials and the curing cross-linked network structure of the SMPN, details of the preparation procedure can be found in our previous work [22]. Fig. 3b compares the normalized FTIR spectra of ground SMPN with that of the exposed SMPN surface. The absorption peaks of isoindoline near 1713 cm^{-1} and phthalocyanine around 1013 cm^{-1} are clearly distinguishable after exposure, although the intensities exhibit a slight decrease. The absorption peak corresponding to the triazine structure at 1519 cm^{-1} and 1355 cm^{-1} still exhibits strong absorption. This indicates that the cross-linked structure of SMPN remains stable, which can be attributed to the high bond energy and robust network formed at high temperature, endowing the resin with excellent resistance to degradation under space environmental exposure. After space exposure, the stretching vibration peak at 2230 cm^{-1} associated with residual–CN groups almost disappear, and the absorption peaks of alkane groups (2800–3000 cm^{-1}) significantly decrease. This observation suggests that segments in SMPN with relatively low bond energies, including $–CH_3$ and residual –CN groups, are preferentially degraded under harsh space environmental conditions.

Further insights are provided by XRD analysis of the sample surface. As shown in Fig. 3c, the main diffraction peaks of the samples before and after exposure are both located at $2\theta = 18–20°$, which is characteristic of

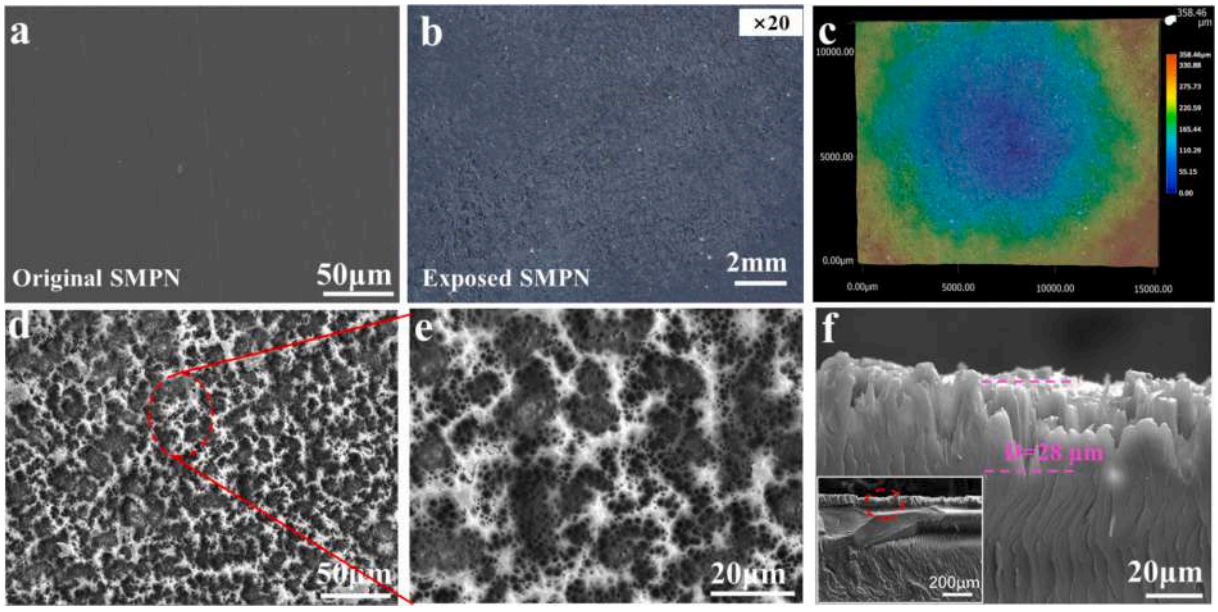

Fig. 2. (a) SEM image of original SMPN surface. (b) Magnified view and (c) 3D ultra depth of field microscope of the exposed SMPN sample. (d-e) SEM image of the surface and (f) SEM image of cross-section of the exposed SMPN sample.

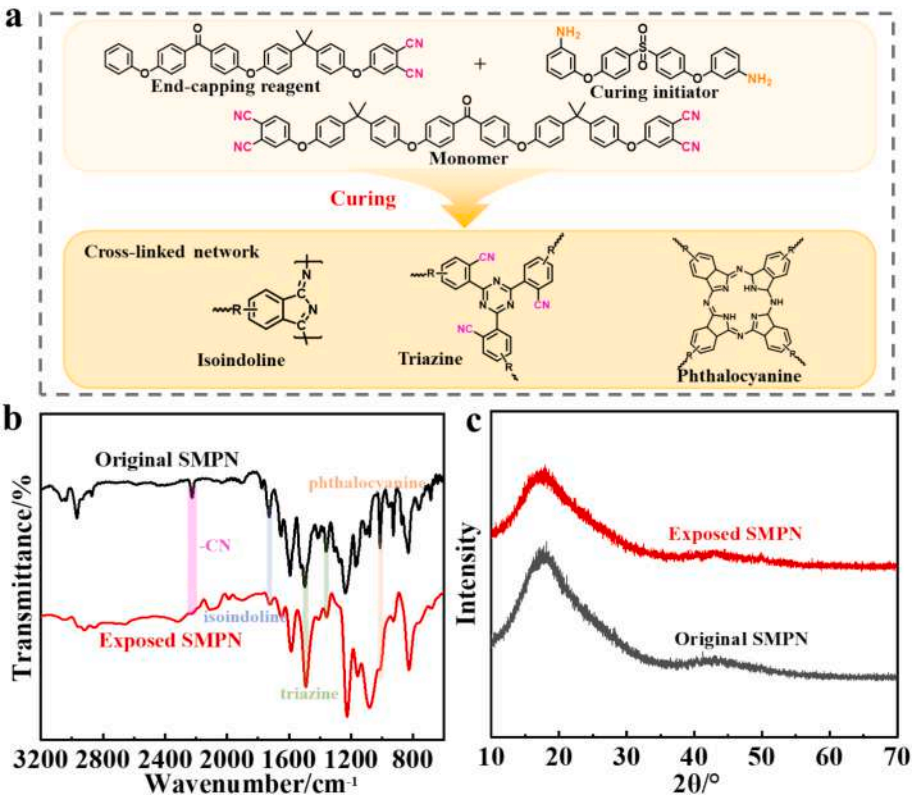

Fig. 3. (a) Monomer structure and cross-linked network structure of SMPN. (b) FTIR spectra of ground and exposed SMPN samples. (c) XRD patterns on the surface of the samples.

amorphous polymer. No peak shift or additional diffraction peaks are observed after exposure, indicating that the polymer chain structure remains stable. However, the primary diffraction peak of the exposed SMPN became broader and less intense, indicating an increase in structural amorphousness, which can be attributed to the scission of alkane segments caused by prolonged space exposure.

The X-ray photoelectron spectroscopy (XPS) was employed to analyze the surface chemical states and bonding information of the SMPN. Since SMPN is a chemically homogeneous resin, a random test point can serve as a reference to represent the bonding energy state of the material. Fig. 4a presents the XPS spectra of C 1s, O 1s, and N 1s for the ground control sample, with the corresponding chemical bonds identified through peak deconvolution. In the C 1s spectrum, in addition to the main peaks assigned to C–C (284.6 eV), C-O-C (286.0 eV), C≡N (286.5 eV), and C=O (287.9 eV), a characteristic π–π* shake-up satellite peak associated with aromatic conjugated structures is observed at 292.4.[24] In the O 1s spectrum, the peaks at 531.3 eV and 533.0 eV are attributed to C–O–C and C=O, respectively. The peak at 399.8 eV in the N 1s spectrum belongs to C≡N. After space exposure, the SMPN surface exhibits mountain like morphologies due to the environmental erosion. To further clarify the evolution of surface chemical characteristics, two positions on the exposed SMPN surface were random selected for analysis. A notable change in the C 1s spectrum is the attenuation of the π–π* shake-up satellite peak, as shown in both Fig. 4b and 4c, indicating the degradation of aromatic conjugated structures, which is associated with the scission of aliphatic segments that disrupts the aromatic network. Moreover, the enhancement of the C–O–C peak and the increase in its integrated area suggest surface oxidation of the SMPN, which can be ascribed to the erosive effect of atomic oxygen in the space environment. The results are also consistent with the O 1s spectrum, which shows a relative increase in the C–O–C component. This increase can be attributed to the destruction of aliphatic segments on the SMPN surface by atomic oxygen. In the N 1s spectrum, the attenuation and disappearance of the C≡N peak at both test points suggests that the nitrile groups were degraded or eliminated due to the combined effects of AO, UV radiation, and high-energy particle bombardment in the space environment, which is consistent with the FTIR analysis. The erosion and damage on the SMPN surface caused by the LEO environment mainly result in enhanced C–O–C component and the breakdown of –CN groups.

3.3. Evolution of mechanical strength and thermal stability

To further evaluate the performance of the space-exposed SMPN, the reduced modulus and hardness were measured using nanoindentation. Fig. 5a and b respectively present the load–displacement curves of the original sample and the exposed sample, and the inset shows the morphology of the test area. Fig. 5c gives the measured reduced modulus and hardness. As the surface of the original SMPN is relatively flat, the five load–displacement curves exhibit highly consistent profiles. In contrast, the curves of the exposed SMPN show significant fluctuations due to surface roughening caused by space-induced erosion. However, the tested reduced modulus of both the original SMPN and the exposed SMPN is at the same level, approximately 4.5 GPa. The hardness of both samples is also comparable, at around 2.3 GPa. On the one hand, the rough surface introduces some interference in the accuracy of the test results for the exposed SMPN. On the other hand, the space environment primarily affects the surface chemical structure and physical morphology of SMPN, without causing significant degradation of its intrinsic physical and chemical properties.

Dynamic Mechanical Analysis (DMA) was used to investigate the thermodynamic behaviors of samples, Fig. 5d and Fig. 5e shows the temperature-dependent storage modulus curves of original and exposed SMPN, respectively. The storage modulus of both samples at room temperature remains at approximately 3000 MPa, and the glass transition temperature (T_g) is around 260 °C. The thermodynamic behavior of the exposed SMPN is comparable to that of the original sample,

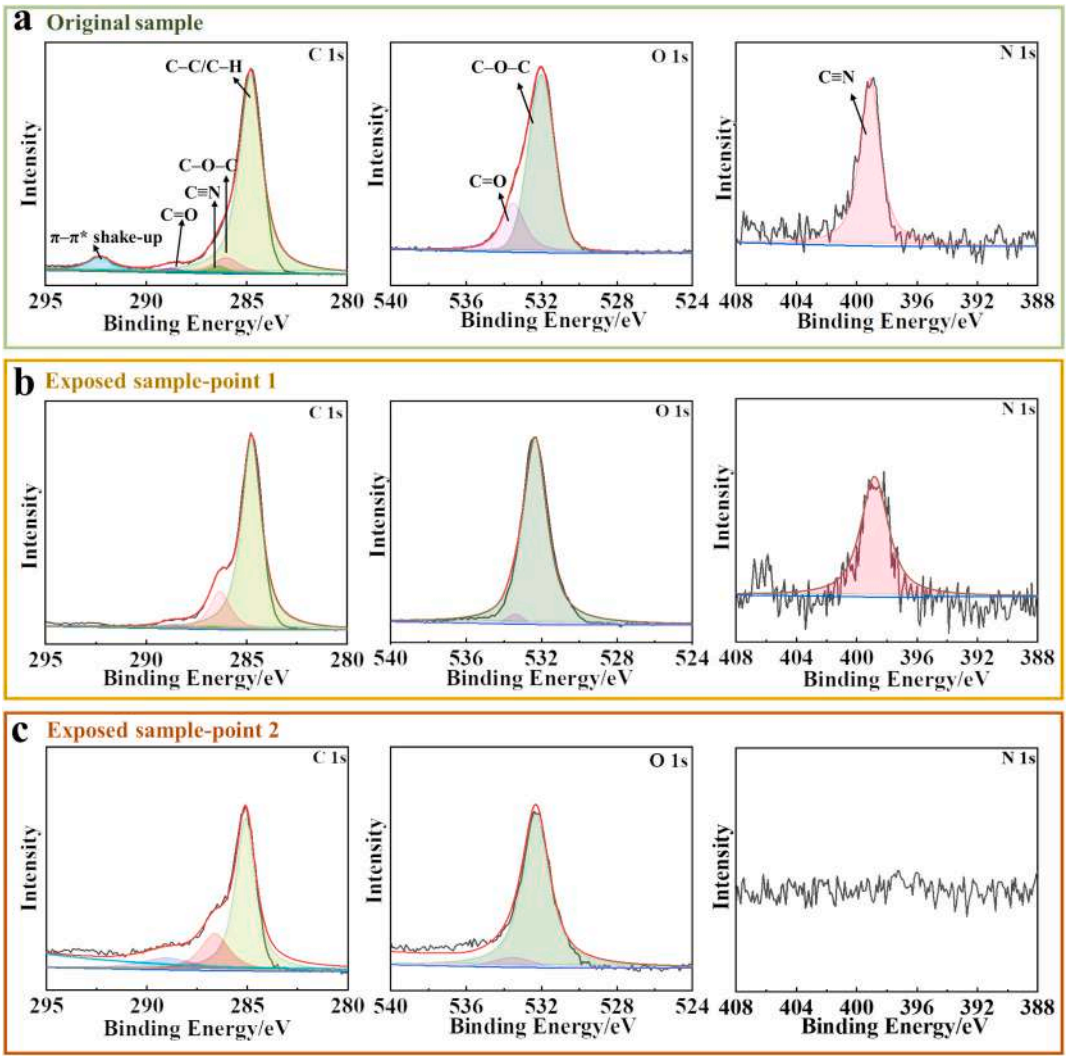

Fig. 4. XPS spectroscopy of (a) ground and (b-c) exposed SMPN samples.

suggesting that one year of space exposure resulted mainly in surface erosion, without significantly affecting the internal properties of the SMPN.

The TGA results also corroborate the above analysis. Fig. 5f shows that the thermal decomposition temperature of exposed SMPN is 418 °C, which is slightly lower than that of original sample. The residual carbon content at 1000 °C of exposed SMPN decreased but remained at a high level, exceeding 57%. The slight decrease in thermal stability can be attributed to the damage of the surface aliphatic segment, which facilitates the escape of small molecules upon heating. Additionally, the microporous structure formed by space erosion further promotes the release of pyrolysis-generated volatiles. However, since the space erosion occurs only on the surface of the SMPN and has not penetrated into its interior, the overall thermal stability remains at a high level.

3.4. Shape memory behavior of exposed SMPN

The shape memory behavior of the exposed SMPN was evaluated using the sample in the temporary "U" shape. Fig. 6a presents the original state of the U-shaped SMPN mounted on the metal substrate, and Fig. 6b illustrates a schematic of the U-shaped SMPN sample during space exposure. The outer surface of the upper section of the U-shaped SMPN faced the flow direction and was subjected to harsher space conditions than other parts. A thermistor was installed on the metal substrate to monitor the ambient temperature, and the temperature during the exposure experiment was maintained between 10 °C and 38 °C, which is far below the T_g of the SMPN (~260 °C). Therefore, as shown in Fig. 6c, the U-shaped SMPN still maintained its temporary shape after exposure. The shape recovery process of the SMPN sample was conducted on a hot plate at 320 ℃. Fig. 6d shows that the temporary "U" shape gradually recovers to its original flat structure after 480 s, achieving a shape recovery rate of approximately 97%. The detailed recovery process is presented in Supporting Video 1. It turns out that the SMPN exposed to the space environment for 1 years still possesses excellent shape memory behavior. This is mainly because the effects of the space environment only cause limited surface damage to the SMPN, without degrading its intrinsic properties.

3.5. Surface morphology analysis of U-shaped SMPN

Owing to its distinctive temporary "U" shape, different regions of the SMPN were subjected to varying degrees of space damage. The digital photos of the outer and inner surfaces of the U-shaped SMPN sample after shape recovery are presented in Fig. 7a and Fig. 7b, respectively. Four distinct regions are clearly observed on the outer surface of the recovery sample and are designated as regions I, II, III and IV. On the inner surface, excluding the area covered by rivets, two distinct regions, designated as region V and region VI, can be identified. The microstructures of these surface regions were further observed by SEM.

On the outer surface, two transition regions are first presented in

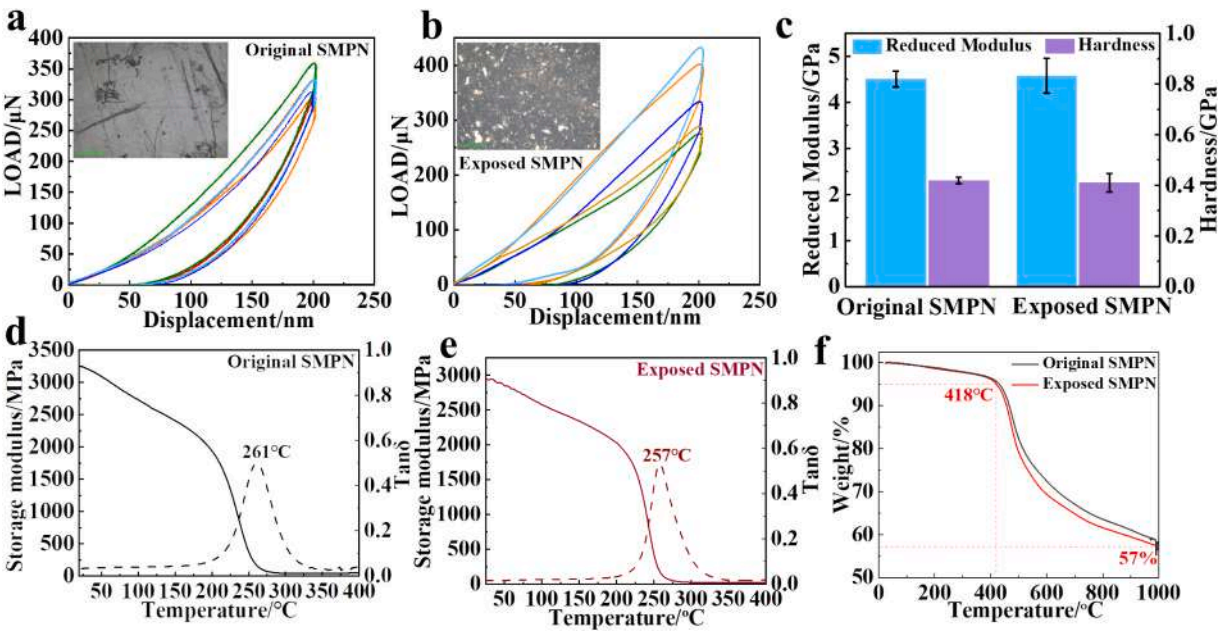

Fig. 5. Nanoindentation test of (a) original and (b) exposed SMPN. (c) Reduced modulus and hardness of nanoindentation test. DMA curves of (a) original and (b) exposed SMPN. (c) TGA curves of original and exposed SMPN.

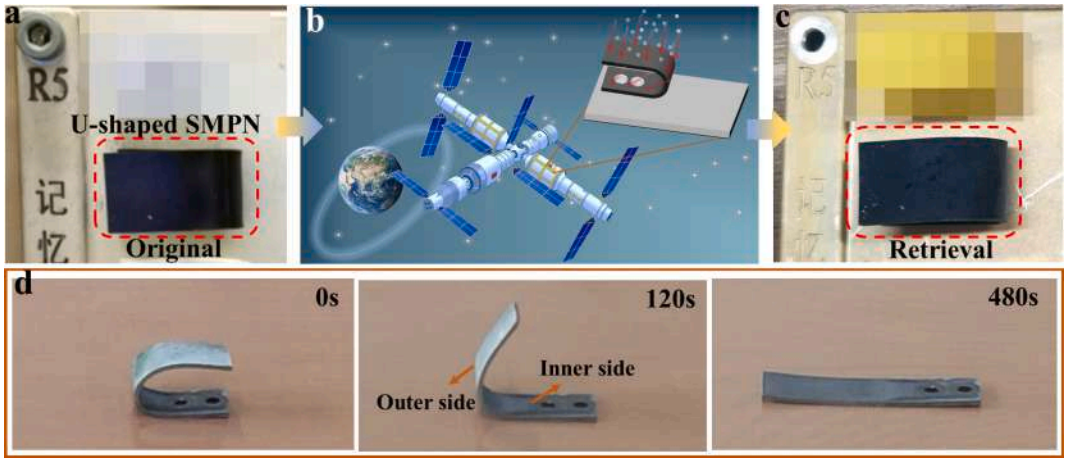

Fig. 6. (a) Digital photo of the original U-shaped SMPN sample. (b) Schematic diagram illustrating the space exposure of the U-shaped SMPN sample. (c) Digital photo of the retrieved U-shaped SMPN sample. (d) Shape recovery process of the exposed SMPN.

Fig. 7c and 7d: one between region I and II, and another between region III and IV. Enlarged images of each region are subsequently provided. The curved surface of the U-shaped sample undergoes varied damage. Since half of the outer surface directly faced the particle flow, Fig. 7e shows that region I suffers severe erosion. Its surface morphology is characterized by a compact array of acicular projections, indicative of typical AO-induced erosion, consistent with surface features observed in AO-eroded polymers aboard the ISS [23]. The erosion in region II is less pronounced than that in region I. Under higher magnification, parallel damage patterns are observed in Fig. 7f, which can be attributed to directional erosion caused by radiation and particle fluxes impinging tangentially on the U-shaped surface. Region III, located beneath region II, was subjected to considerably less radiation and erosion due to the shielding provided by region II, and therefore experienced relatively mild damage. As shown in Fig. 7g, its surface mainly exhibits shallow gully-like morphology, without deep erosion. Fig. 7h shows that region IV only exhibits a slightly rougher surface compared with the original morphology shown in Fig. 2a, which can be attributed to its close contact with the metal substrate and therefore minimally affected by the space environment.

At the inner side, region V, mainly positioned on the backlit side of region I, did not undergo direct radiation and was primarily affected by secondary environmental factors such as diffused atomic oxygen and charged particles. The blackened region VI in Fig. 7b is believed to result from oblique irradiation and particle flow impacting the inner surface during orbital cycles, when the spacecraft orientation allowed partial exposure of inner areas. Fig. 7i shows the transition zone between regions V and VI, with a more indistinct boundary than other transition regions, which can be attributed to the scattered radiation acting on region VI during the orbital cycle of the space station. Under higher magnification, region V exhibits pronounced surface cracking (Fig. 7j) due to diffuse AO and high-energy particle impact, whereas region VI shows directional erosion patterns (Fig. 7k), resulting from particle flux aligned with the orbital flow direction.

Another transition region is observed on the inner surface between region VI and the area beneath the mounted rivets, as shown in Fig. 7l. A

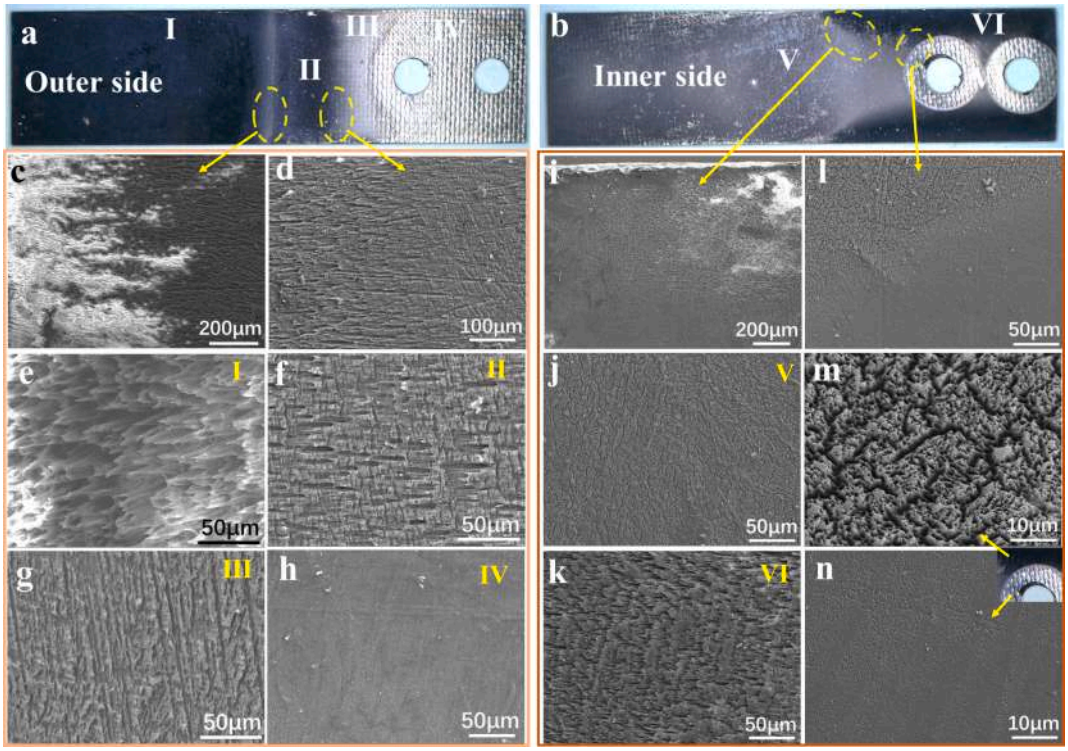

Fig. 7. Digital photographs of (a) the outer surfaces and (b) the inner surfaces of the recovered SMPN. (c-h) SEM images of different regions on outer surface. (i-n) SEM images of different regions on inner surface.

clear boundary can be identified due to the shielding effect of the rivets. The high magnification SEM image in Fig. 7m shows that the area of region VI near the rivets exhibits not only surface crack but also numerous micropores, similar to those observed in Fig. 2e, indicating that the spatial corrosion in this area is more severe. This is primarily because the region is located at the edge of the U-shaped shielding, where it is more susceptible to the influence of space environmental factors such as AO and UV radiation. Beneath the rivet, the area sustains only minor damage, and the surface remains relatively smooth (Fig. 7n). Actually, both the outer and inner surfaces of the exposed U-shaped SMPN exhibit gradient damage, potentially offering valuable insights for the optimization of spacecraft structural designs against environmental degradation.

FTIR was employed to characterize the structural variations across the outer and inner surface. As shown in the inset images of Fig. 8, three positions were selected for testing on each side, and the corresponding curves are labeled P1 through P6. The obtained FTIR curves were normalized to allow for precise comparison. Fig. 8a shows that the spectrum of P3 on the outer surface is nearly identical to that of the ground sample, due to its adhesion to the metal substrate and consequent protection from space exposure. The absorption peak of P1 is similar to that of the exposed flat SMPN. Distinct absorption peaks corresponding to cross-linked structures, such as triazine at 1519 cm^{-1} and 1355 cm^{-1}, are observed clearly. The −CN groups (~2230 cm^{-1}) and aliphatic segments (2800–3000 cm^{-1}) show reduced intensity, indicating the impact of space irradiation on this region. P2 was selected from the transition region of irradiation, and the corresponding absorption peaks of aliphatic segments and −CN groups exhibit intermediate intensity compare with those of P1 and P3. On the inner side, as shown in Fig. 8b, the absorption peaks associated with the cross-linked structure of SMPN remain prominent, whereas the absorption of −CN groups near 2230 cm^{-1} is attenuated in the tested regions. This suggests that even on the backside of the windward side, SMPN undergoes surface structural damage, which can be attributed to diffuse AO and

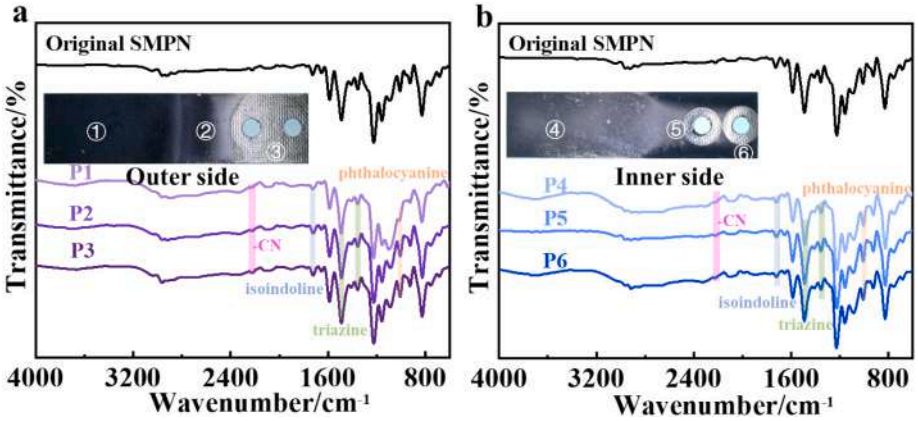

Fig. 8. FTIR spectra from different regions on (a) outer surface and (b) inner surface.

charged particles and so on. The effects of different space environmental factors on SMPN will be further explored in our future studies.

3.6. Carbon fiber reinforced composites

In practical applications, resin materials are often reinforced through composite techniques to enhance their properties. Hence, the composite of SMPN and CF was prepared, with composites containing 1, 2, and 3 layers of CF named as SMPNC1, SMPNC2, and SMPNC3, respectively. The corresponding composite thicknesses were 0.48 mm, 0.62 mm, and 0.91 mm. All samples were cut along the ±45° direction relative to the carbon fabric. The tensile stress–strain curves are shown in Fig. 9a. After composite reinforcement, the material strength is significantly improved. The tested SMPNC2 exhibits the best tensile performance, with a breaking strength of approximately 200 MPa at an elongation of 1.7%, which far exceeds that of the pure SMPN. Fig. 9b shows the flexural stress–strain curves of the composites. The single-layer composite SMPNC1 exhibits almost no improvement in bending performance compared to SMPN, as the fibers are not aligned with the primary loading direction, and the bending load is mainly borne by the SMPN matrix. As the number of CF layers increases, the resulting thickness enhancement leads to higher strength and more effective stress distribution, thereby significantly improving the flexural performance of the composites. SMPNC2 exhibits a flexural strength exceeding 300 MPa, while that of SMPNC3 decreases. This reduction is not due to a loss in material strength, but rather results from the increased thickness of SMPNC3, which lowers the calculated bending strength. Fig. 9c presents the corresponding tensile and flexural modulus of SMPNC. When the number of CF layers exceeds two, both the tensile and flexural modulus are significantly enhanced, indicating that the SMPNC possesses greater load-bearing capacity and stability, thereby improving its safety and reliability.

The fracture morphology of SMPNC tensile specimens was analyzed via SEM to investigate the failure mechanisms of the composite. Fig. 9d shows that the cross-section of SMPNC1 appears relatively flat, with good interfacial bonding between the carbon fibers and the resin. Minimal plastic deformation and fiber pull-out are observed, indicating a predominantly brittle fracture behavior. The cross-section of SMPNC2 is rough and shows signs of interlayer separation (Fig. 9e). The composite exhibits a complex failure mode involving fiber fracture, matrix cracking, and interfacial debonding. It can be seen from Fig. 9f that the fracture surface of SMPNC3 exhibits prominent voids and interlayer separation. In some areas, CFs have detached from the matrix, forming large pores. The main failure modes are interfacial debonding and delamination. An increase in the number of layers leads to more complex tensile fracture behavior in SMPNC, primarily due to the development of complex stress gradients and shear stress concentration zones between layers during the tensile process of multilayer structures. When the interfacial bonding is weak, these stress concentrations readily lead to interlayer debonding or delamination cracks. In subsequent research, comprehensive investigations will be conducted on interface modification of fiber-reinforced SMPN composites to further enhance their mechanical performance.

With the composition of CF, SMPNC can be processed into complex structures and still exhibits excellent shape memory properties. A 30 × 30 × 30 mm^3 square box with a thickness of approximately 0.55 mm was prepared using SMPNC2. It can be fixed either in a sheet configuration unfolded outward by 90° or in a folded structure bent inward by 90°. The shape recovery processes of both temporary shapes are shown in Fig. 10a and Fig. 10b. Upon thermal stimulation, the temporary shapes gradually recovered to its original three-dimensional shape, with detailed recovery process provided in Supporting Video 2 and 3. The sheet configuration exhibits a smooth and gradual shape recovery to its original shape under thermal stimulation. In the folded temporary shape, heat transfer at the bottom is uniform. When the deformation temperature is reached, the release of stored energy on the inner folding surface is constrained by the outer surface. With the gradual recovery of the outer surface and the buildup of resilience in the inner surface, the release of stored energy leads to the shape recovery of the original box shape. The transformation of SMPNC from a two-dimensional to a three-dimensional structure can substantially enhance its value for spatial applications. And the integration of space-environment adaptability, stimuli-responsiveness, and enhanced mechanical strength endows SMPNC with great potential as a smart material for aerospace structures.

4. Conclusions

In this work, the damage to SMPN in the LEO environment was

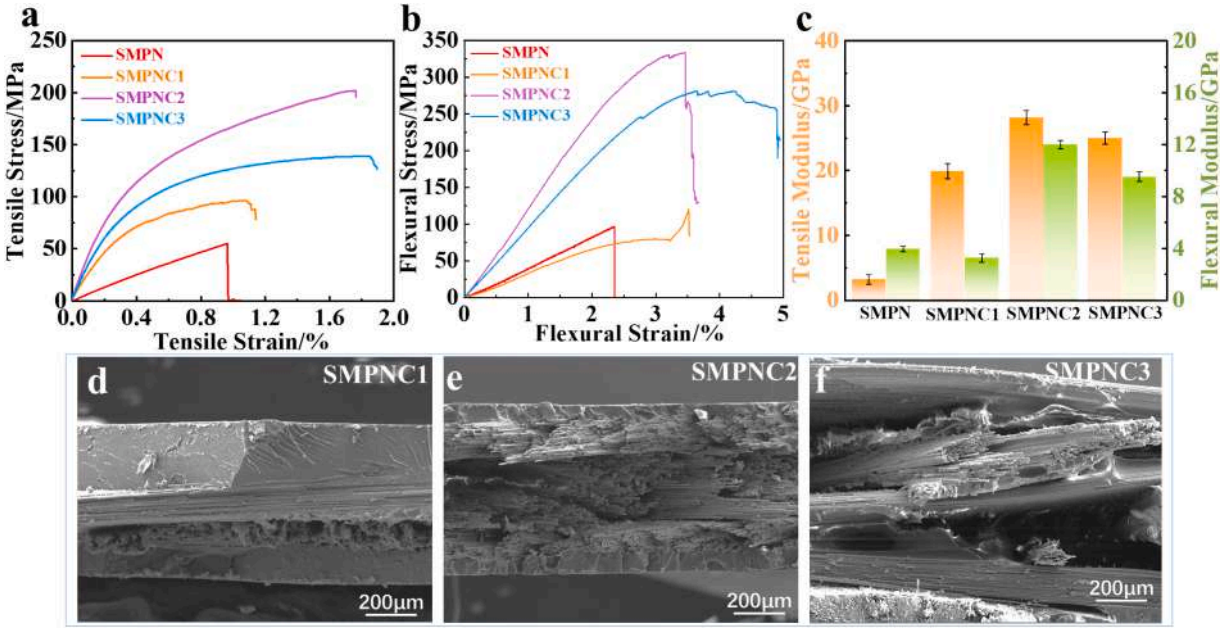

Fig. 9. (a) Tensile stress–strain curves and (b) flexural stress–strain curves of SMPNC. (c) Tensile and flexural modulus of SMPNC. (d-f) Fracture morphology of SMPNC tensile specimens.

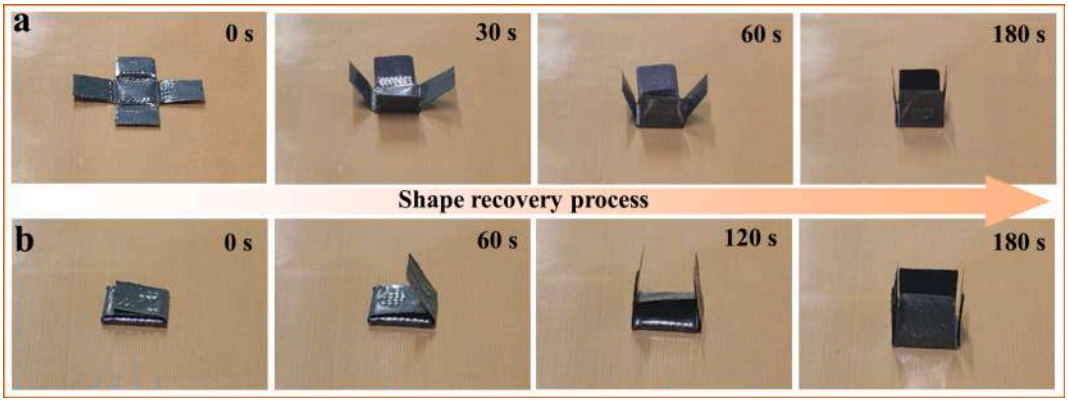

Fig. 10. Shape recovery process of a square SMPNC box from temporary shapes: (a) an outward unfolded sheet and (b) an inward folded structure.

revealed for the first time. After being exposed on the CSS for 1 years, the mass loss ratio of the SMPN remains around 6%, primarily due to surface erosion. SEM reveals that the exposed surface of the SMPN exhibits a dense microporous structure, with an erosion depth of up to 28 μm. FTIR results of the exposed SMPN surface demonstrate the degradation of aliphatic segments and −CN groups, while the cross-linked structure remains comparatively stable. Nanoindentation, DMA, TGA tests indicate that the functional properties of the SMPN were not substantially affected. The exposed SMPN with a temporary "U" shape was still able to recover to its original shape upon thermal stimulation. Since its shape memory performance remained unaffected after exposure, SMPN can be considered a space-qualified smart material. The systematic investigation of surface morphologies in the shape recovery SMPN indicates that the curved surface of the U-shaped sample undergoes gradient damage, which could inform the optimization of damage-resistant designs in spacecraft structures. CF-reinforced SMPN composites exhibit significantly enhanced mechanical properties while retaining shape memory performance, making them promising candidates for deployable aerospace structures.

CRediT authorship contribution statement

Rongxiang Hu: Writing – original draft, Investigation. **Fenghua Zhang:** Writing – review & editing, Funding acquisition. **Yanju Liu:** Funding acquisition. **Liwu Liu:** Project administration, Funding acquisition. **Zhengxian Liu:** Project administration. **Jinsong Leng:** Supervision, Resources.

Declaration of competing interest

The authors declare that they have no known competing financial interests or personal relationships that could have appeared to influence the work reported in this paper.

Acknowledgments

This work was financially supported by the National Natural Science Foundation of China (Grant No. 92271112 and No. 92271206) and the Space Utilization System of China Manned Space Engineering (Grant No. KJZ-YY-WCL06). The authors would like to thank the support of the Chinese astronauts for performing all the space experiments.

Appendix A. Supplementary material

Supplementary data to this article can be found online at https://doi.org/10.1016/j.compositesa.2026.109641.

Data availability

Data will be made available on request.

References

[1] Xia Y, He Y, Zhang F, Liu Y, Leng J. A review of shape memory polymers and composites: mechanisms, materials, and applications. Adv Mater 2021;33(6). https://doi.org/10.1002/adma.202000713.
[2] Ni C, Chen D, Yin Y, Wen X, Chen X, Yang C, et al. Shape memory polymer with programmable recovery onset. Nature 2023;622(7984):748-+. https://doi.org/10.1038/s41586-023-06520-8.
[3] Liu Y, Wang L, Liu Y, Zhang F, Leng J. Recent progress in shape memory polymer composites: driving modes, forming technologies, and applications. Compos Commun 2024;51. https://doi.org/10.1016/j.coco.2024.102062.
[4] Yan S, Zhang F, Luo L, Wang L, Liu Y, Leng J. Shape memory polymer composites: 4D printing, smart structures, and applications. Research 2023;6. https://doi.org/10.34133/research.0234.
[5] Sun J, Peng B, Lu Y, Zhang X, Wei J, Zhu C, et al. A photoorganizable triple shape memory polymer for deployable devices. Small 2021;18(9). https://doi.org/10.1002/smll.202106443.
[6] Liu Y, Du H, Liu L, Leng J. Shape memory polymers and their composites in aerospace applications: a review. Smart Mater Struct 2014;23(2). https://doi.org/10.1088/0964-1726/23/2/023001.
[7] Li F, Liu Y, Leng J. Progress of shape memory polymers and their composites in aerospace applications. Smart Mater Struct 2019;28(10). https://doi.org/10.1088/1361-665X/ab3d5f.
[8] Angirasa D, Ayyaswamy PS. Review of evaluation methodologies for satellite exterior materials in low earth orbit. J Spacecr Rocket 2014;51(3):750–61. https://doi.org/10.2514/1.A32742.
[9] Tan Q, Li F, Liu L, Liu Y, Yan X, Leng J. Study of low earth orbit ultraviolet radiation and vacuum thermal cycling environment effects on epoxy-based shape memory polymer. J Intell Mater Syst Struct 2019;30(18–19):2688–96. https://doi.org/10.1177/1045389x19873398.
[10] Jayalath S, Herath M, Epaarachchi J, Trifoni E, Gdoutos EE, Fang L. Durability and long-term behaviour of shape memory polymers and composites for the space industry - a review of current status and future perspectives. Polym Degrad Stab 2023;211. https://doi.org/10.1016/j.polymdegradstab.2023.110297.
[11] Santo L, Quadrini F, Bellisario D, Iorio L, Proietti A, de Groh KK. Effect of the LEO space environment on the functional performances of shape memory polymer composites. Compos Commun 2024;48. https://doi.org/10.1016/j.coco.2024.101913.
[12] Plis EA, Badura G. The spectral characterization of novel spacecraft materials in the low earth orbit environment. J Astronaut Sci 2024;71(2). https://doi.org/10.1007/s40295-024-00436-9.
[13] Plis EA, Bengtson MT, Engelhart DP, Badura GP, Cowardin HM, Reyes JA, et al. Ground testing of the 16th materials international space station experiment materials. J Spacecr Rocket 2023;60(2):385–90. https://doi.org/10.2514/1.A35502.
[14] Di Trani N, Masini A, Bo T, Paci MM, Batra JS, Reggiani M, et al. Probing physicochemical performances of 3D printed carbon fiber composites during 8-month exposure to space environment. Adv Funct Mater 2023;34(13). https://doi.org/10.1002/adfm.202310243.
[15] Yamagishi A, Hashimoto H, Yano H, Imai E, Tabata M, Higashide M, et al. Four-year operation of tanpopo: astrobiology exposure and micrometeoroid capture experiments on the JEM exposed facility of the international space station. Astrobiology 2021;21(12):1461–72. https://doi.org/10.1089/ast.2020.2430.
[16] Rejsek-Riba V, Inguimbert V, Duzellier S, Pons C, Crepel M, Tighe AP. Spectrometers results of material exposure and degradation experiment onboard international space station. J Spacecr Rocket 2011;48(1):38–44. https://doi.org/10.2514/1.49443.

[17] Kimoto Y, Yano K, Ishizawa J, Miyazaki E, Yamagata I. Passive space-environment-effect measurement on the international space station. J Spacecr Rocket 2009;46(1):22–7. https://doi.org/10.2514/1.31851.
[18] Li L, Zhang G, Zhang H, Xiao Y, Zhao S, Song J, et al. Transport of volatiles in agglutinates from lunar Regolith of chang'e-5 mission. Research 2025;8. https://doi.org/10.34133/research.0638.
[19] Zhang X, Liu Y, Zhao S, Song J, Yao W, Wang W, et al. Melting and rapid solidification of lunar regolith particles returned by Chang'E-5 mission. Research 2024;7. https://doi.org/10.34133/research.0486.
[20] Liu D, Wang H, Liao H, Chang J, Wei B. Wrinkled shrinkage on surface monophasic structure of floating refractory alloy droplets solidified in space environment. Adv Funct Mater 2025;35(7). https://doi.org/10.1002/adfm.202415364.
[21] Wang H, Liao H, Hu L, Zheng C, Chang J, Liu D, et al. Freezing shrinkage dynamics and surface dendritic growth of floating refractory alloy droplets in outer space. Adv Mater 2024;36(24). https://doi.org/10.1002/adma.202313162.
[22] Hu R, Zhang F, Luo L, Wang L, Liu Y, Leng J. An end-capping strategy for shape memory phthalonitrile resins via annealing enables conductivity and wave-absorption. Chem Eng J 2024;489. https://doi.org/10.1016/j.cej.2024.150956.
[23] de Groh KK, Banks BA, Miller SKR, Dever JA. Degradation of spacecraft materials. Handbook of Environmental Degradation of Materials 2018:601–45. https://doi.org/10.1016/b978-0-323-52472-8.00029-0.
[24] Morgan DJ. Comments on the XPS analysis of carbon materials. C 2021;7(3). https://doi.org/10.3390/c7030051.